



PERGAMON

Neural Networks 14 (2001) 645–656

Neural  
Networks

www.elsevier.com/locate/neunet

2001 Special issue

## Space-rate coding in an adaptive silicon neuron

Kai Hynna\*, Kwabena Boahen

*Penn Bioengineering, 3320 Smith Walk, Philadelphia, PA 19104-6392, USA*

Accepted 22 January 2001

### Abstract

Neurophysiology is largely the study of spike rates of single neurons, under controlled conditions, with the hope that these results reflect how populations of neurons compute. However, the population response differs radically from the single-neuron response if the membrane voltage's rate of change drops dramatically when it is close to the spike-firing threshold. By delaying spiking, this slew-rate adaptation has been shown to regulate spike rate and prolong synaptic integration at the single-neuron level. We show here that it sharpens sensitivity and shortens latency at the population level. Thus, slew-rate adaptation enables neurons to process information faster than their interspike interval by using space-rate coding, instead of time-rate coding. This study also suggests how neural populations can modulate their gain and synchrony by regulating active conductances. Our results are extrapolated from experiments and analysis performed on a single silicon neuron, with Ca- and voltage-dependent potassium-channel analogs. © 2001 Elsevier Science Ltd. All rights reserved.

### 1. Space-rate coding

The question of information encoding in the brain is still one of much debate. For many years, the idea that stimuli were encoded in the mean firing rate of a neuron dominated, with downstream neurons averaging their inputs temporally to read this code. However, humans can process information on a timescale of a few hundred milliseconds (Thorpe, Fize, & Marlot, 1996), and with neurons firing at an average rate of 10 Hz, processing through multiple layers seems impossible using a mean rate code. Evidently, a faster method of computation must be used.

More recently, evidence that stimuli are encoded by actual spike timing, relative to another signal (stimulus, intrinsic oscillation, or other inputs, Gerstner, 1999), is accumulating. Neurons have demonstrated the ability to accurately reproduce their spike trains to a time varying input (Buracas, Zador, DeWeese, & Albright, 1998; Mainen & Sejnowski, 1995). Synchronous firing between neurons, one form of temporal coding, can encode more information collectively than individually (Dan, Alonso, Usrey, & Reid, 1998) as well as provide stronger input to downstream neurons (Alonso, Usrey, & Reid, 1996). Thus, information need not be encoded in the activity of a single neuron, but may be represented in the collective activity of a population of neurons. This distributed representation is called *popula-*

*tion coding* (deCharms & Zador, 2000) or *space-rate coding* (Maass & Natschlagler, 2000).

Models that abstract a spike train into an analog rate variable do not capture fast transients in the population activity due, for example, to synchrony. These fast transients can be reproduced by a simple integrate-and-fire model of spike generation. However, integrating current on a capacitor produces a linear membrane voltage trajectory. As a consequence, the distribution of neurons between reset and threshold is uniform. However, real neurons have other active conductances—apart from the spike-generating ones—that can alter this uniform distribution by reshaping the membrane voltage trajectory. In this paper, we demonstrate how this redistribution leads to efficient space-rate coding using an adaptive silicon neuron that includes active conductances.

In particular, our neuromorphic model includes two types of active conductances, both of which arise from ion channels (pores) in the cell membrane that are permeable to potassium ions (K). These channels reduce the rate of change of the membrane voltage by shunting current out of the cell, thereby throttling the spike rate. The K channels that we model open when the membrane voltage rises or when the internal calcium (Ca) concentration increases. These types of K channels are simply called voltage-dependent and Ca-dependent channels, respectively.

Active membrane behavior was modeled in silicon in

\* Corresponding author.

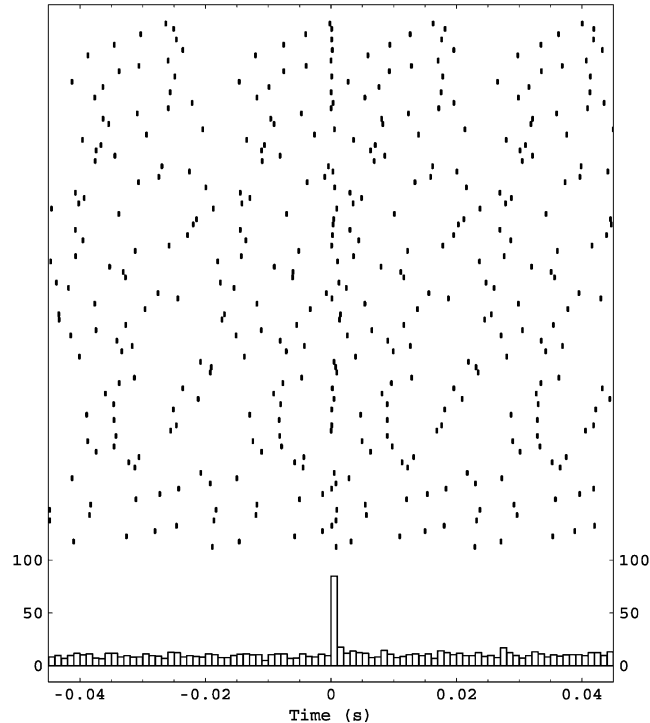


Fig. 1. Spike rasters. Spike trains recorded from AdaptSiNeuron in 100 trials, selected at random from a total of 700, in response to a 5.2% step change in input current. A histogram of all 700 trials is shown below the raster plot; 1 ms bins were used. Step inputs were generated by applying a square wave (between 1 and 10 Hz) from an HP33120A function generator through a 20 M $\Omega$  resistor. This current was supplied through a pMOS current mirror, formed by a 460/6 (width/length in micrometers) diode-connected transistor in the pad and a 6/12 transistor in the circuit—a step-down ratio of 153. The initial current level was 2.06 nA for this and all subsequent runs. Latencies were measured with an HP55131A counter under computer control.

Mahowald and Douglas (1991) where spike rate adaptation in a neocortical pyramidal cell was reproduced by building Ca- and voltage-dependent K channel analogs. In this previous work, an analogy was made between a transistor and an ion channel, and differential (transconductance) amplifiers were used to realize active behavior. We have developed a simpler, analytically tractable, circuit model by abstracting the spike-generation process and using a simple two-transistor circuit to model the K-channel population as well as the internal Ca concentration. Our K-channel analog has both a fast voltage dependence and a slow Ca dependence.

The remainder of the paper is organized as follows. We describe the effects of Ca- and voltage-dependent K channels in Section 2, and present circuit analogs of these channels in Section 3, where we describe our adaptive silicon neuron. We present our single-neuron experimental measurements, with theoretical fits, in Section 4, and extrapolate the responses of a population of identical neurons from them. For a more analytical treatment, we refer the reader to Appendices A–D, where we present simple, intuitive, derivations of AdaptSiNeuron’s diode-capacitor dynamics, K-current and membrane-voltage trajectories, spike- and slew-rate adaptation factors, and spike probability density, respectively. We conclude the paper with a discussion in Section 5.

## 2. Voltage- and Ca-dependent ion channels

A neuron that lacks passive or active conductances—except for spike-generating ones—simply integrates input current on its membrane capacitance, its membrane voltage increasing (slewing) at a rate proportional to the current level. This slew rate is constant if the current is fixed. In that case, we are equally likely to find the membrane voltage at any point between its reset and threshold levels. Thus, when we step the input current of a population of these neurons, their spike latencies will be distributed uniformly between 0 and  $T$ , the interspike interval. Hence, the spike probability density is  $1/T$ , and we must increase the current by 100% to double it. The median latency, which tells us how long we must wait for half the population to fire, is  $T/2$ . The sensitivity and latency of these ‘Integrate&Fire’ neurons can be improved—without increasing their steady-state spike rate—by adding active conductances, as shown in Fig. 1.

A neuron with voltage-dependent K channels rapidly increases its membrane voltage after its spike is reset, but charges more slowly as it approaches threshold, as shown in Fig. 2a. In this way, its sensitivity and latency improve by the ratio between the slew rate at the beginning and the end of the interspike interval, which we define as the slew-rate adaptation factor,  $\xi$ . Slew-rate adaptation, we propose, is

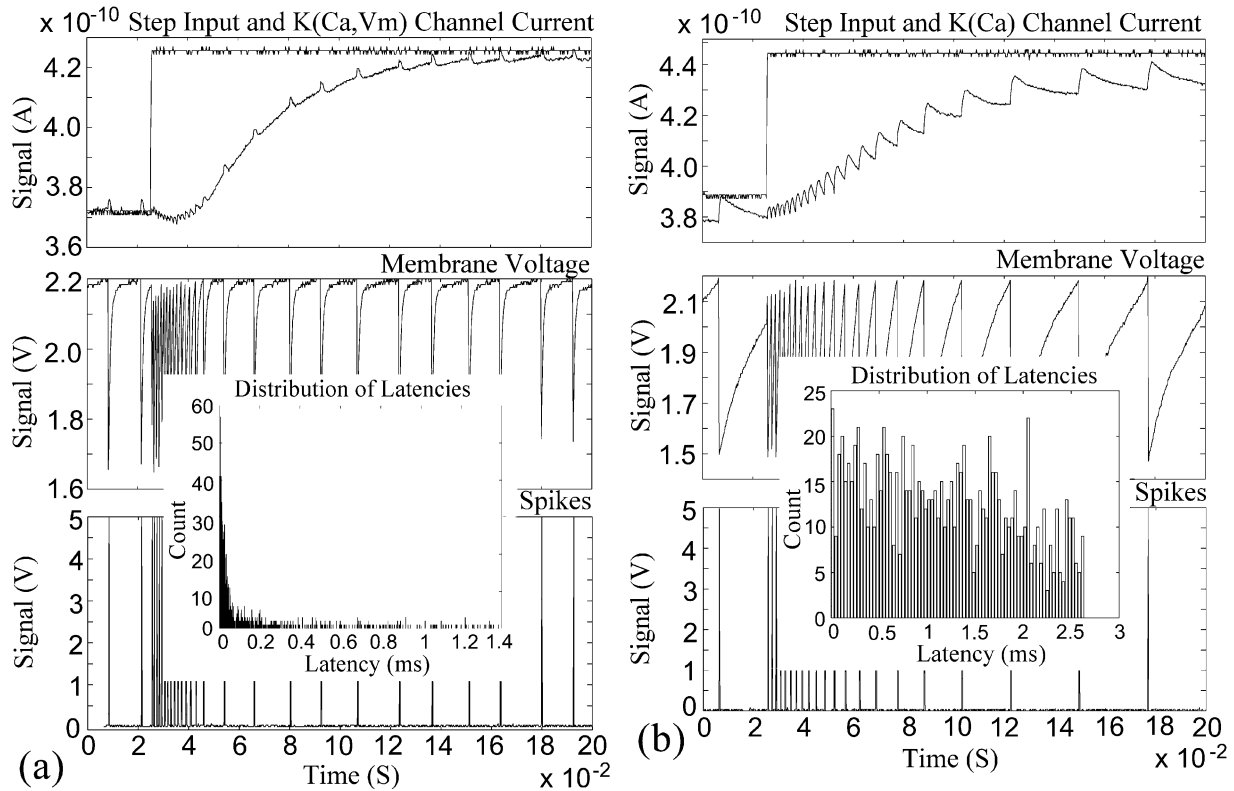


Fig. 2. Slew-rate and spike-rate adaptation. (a) Ca- and voltage-dependent K channels. Top: K current shunted from the input builds up each time the neuron spikes, modeling its Ca dependence—the electrometer cannot follow the fast voltage dependence. Middle: membrane voltage charging from reset (1.5 V) to threshold (2.2 V), driven by the surplus current. Bottom: spikes generated each time the membrane voltage reaches threshold. The first spike’s median latency (insert) was 40  $\mu$ s—32.5 times shorter than the 1.4 ms interspike interval immediately after the step, which is itself 11.4 times shorter than the 16 ms steady-state interspike interval. (b) Voltage-dependence blocked. The membrane voltage repolarizes slowly because the K current does not shut off when the neuron is reset. The median latency (insert) increased to 1.3 ms—half as long as the 2.63 ms interspike interval immediately after the step, which is itself 10 times shorter than the 26 ms steady-state interspike interval. The bias voltages (see Fig. 4a) were  $V_A = 0.350$  V,  $V_{qa} = 4.52$  V,  $V_{mpd} = 1.1$  V,  $V_{pu} = 3.41$  V,  $V_{dd} = 5.0$  V and  $V_{cas} = 4.01$  (a) or 1.35 V (b). A 13.5% change in input current was made in both cases.

due to fast, low-threshold, voltage-dependent potassium channels (Connor & Stevens, 1971; Storm, 1988), which shut off when the membrane voltage drops, leaving surplus input current to repolarize it, and come on as the membrane voltage rises, arresting it. When this voltage dependence is blocked, slew-rate adaptation disappears, as shown in Fig. 2b.

A neuron with Ca-dependent K channels responds to a large increase in its input current with a high-frequency burst, but fires at a much lower rate after it adapts to the new input level, as shown in Fig. 2b. In this way, its sensitivity and latency improve by the ratio between the spike rate immediately after the step and the rate in steady state, which we define as the spike-rate adaptation factor,  $\gamma$ . Spike-rate adaptation has been shown to depend on Ca accumulation in the cell and Ca-dependent K channels (Madison & Nicoll, 1982), which subtract out the short-term temporal average of the input activity. When both voltage- and Ca-dependent channels are present, slew-rate adaptation plays a role in spike-rate adaptation, as reducing the slew rate lengthens the interspike interval.

### 3. Silicon neuron

A block diagram of AdaptSiNeuron, our silicon neuron model, is shown in Fig. 3a. The integrator’s output, which represents the intracellular Ca concentration, adjusts the conductance of the Ca-dependent K-channel analog. This feedback loop adapts the spike rate. The differentiator’s output, which tracks rapid changes in membrane potential, also modulates the K-channel analog. This feedback loop adapts the slew rate. The two-transistor current-mirror integrator shown in Fig. 3b serves as a voltage- and Ca-dependent K-channel analog, and also models the intracellular Ca concentration (Boahen, 1997). Its dynamics, which are analyzed in Appendix A, are evident in the step responses plotted in Fig. 3c and d. For subthreshold MOS transistor operation,  $I_K$  increases exponentially with the Ca-node voltage,  $V_{Ca}$ , which is capacitively coupled to the membrane voltage  $V_m$ . In fact,  $I_K = I_{ds0} \exp(\kappa V_{Ca}/U_T)$ , where  $U_T \equiv kT/q$  is the thermal voltage (25 mV at room temperature) and  $\kappa$  is the subthreshold slope coefficient (typically between 0.6 and 0.8) (Mead, 1989).

Due to the model K current’s joint dependence on

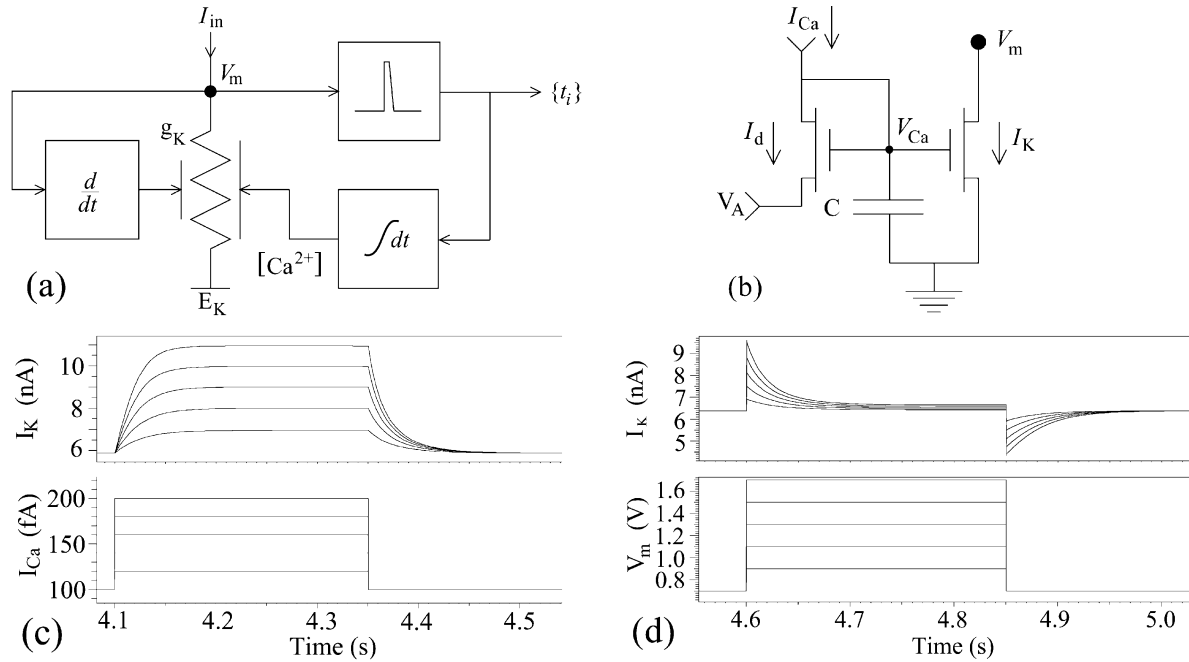


Fig. 3. Modeling K (Ca,  $V_m$ ) channels in silicon. (a) A pulse generator models the axon–hillock while a variable conductance, modulated by a spike integrator and a voltage differentiator, models Ca- and voltage-dependent K channels. (b) Charge on a capacitor,  $C$ , represents intracellular Ca;  $I_{Ca}$  represents current through voltage-dependent Ca channels that open each time a spike occurs, while  $I_d$  represents Ca removal by buffering or pumping. The drain-gate overlap capacitance of the output transistor, which couples  $V_{Ca}$  to  $V_m$ , models the membrane-voltage differentiator. The bias voltage,  $V_A$ , sets the current mirror's gain  $A \equiv \exp(V_A/U_T)$  (i.e.  $I_K/I_d$ ). (c) Step changes reveal a slow but sustained dependence of  $I_K$  on  $I_{Ca}$ , with a time constant of about 20 ms for  $I_{Ca}$  current levels in the 100 fA range. (d) Step changes reveal a fast, but transient, dependence of  $I_K$  on  $V_m$ , with the same time constant, and a small passive conductance. In this simulation, the current-mirror's transistors were identically sized, at  $8 \times 8 \mu\text{m}$ , and  $V_A = 0.3 \text{ V}$ ; the technology was  $1.6 \mu\text{m}$ , n-well, CMOS. There was no explicit integration capacitor (i.e.  $C = 0$ ); the transistor's gate capacitances played this role.

membrane voltage and Ca concentration, this current reaches steady state when the membrane voltage's slew rate balances the Ca concentration's decay rate. As the leaky integrator's time constant is relatively long, the membrane voltage homes in on threshold slowly. Separate voltage- (e.g. the  $I_A$  current, Connor & Stevens, 1971) and Ca-dependent (e.g. the  $I_{AHP}$  current, Lancaster & R, 1986) channel populations would produce qualitatively the same behavior, with channel inactivation augmenting the role of Ca decay. However, Ca dependence extends the operating range by dynamically regulating the K conductance to match the input current level. Hence, this adaptive behavior keeps the membrane voltage just below threshold independent of current level.

AdaptSiNeuron's behavior is described by two simultaneous differential equations, which we derived by applying Kirchoff's current law to the membrane-voltage node and to the Ca-integration node:

$$C_m \frac{dV_m}{dt} = I_{in} - \left(1 + \frac{r_{mc}}{A}\right) I_K - (Q_{th} - r_{mc} q_{Ca}) \delta(t - t_n), \quad (1)$$

$$C_{Ca} \frac{dV_{Ca}}{dt} = r_{cm} (I_{in} - I_K) + (q_{Ca} - r_{cm} Q_{th}) \delta(t - t_n) - \frac{1}{A} I_K, \quad (2)$$

where  $t_n$  is the spike time (i.e. when  $V_m$  equals  $V_{th}$ ). The actual circuit is shown in Fig. 4; it uses the axon–hillock circuit (i.e. spike generator) described in Mead (1989).  $C_m$  and  $C_{Ca}$  are the equivalent node capacitances, and  $r_{mc}$  and  $r_{cm}$  give the fraction of the charge dumped on node  $V_{Ca}$  that goes to node  $V_{mem}$ , and vice versa;  $\delta(\cdot)$  is the unit impulse.  $Q_{th}$  is the charge subtracted from the membrane capacitor on reset and  $q_{Ca}$  is the charge added to the Ca-integration capacitor each time a spike occurs;  $A$  is the current-mirror's gain.

Eq. (1) captures the dependence of the membrane voltage on the input current and on the K-channel current. We have lumped the fast Na current and the delayed-rectifier K current, responsible for generating spikes (Hodgkin & Huxley, 1952), into a net repolarization charge,  $Q_{th}$ , that is subtracted from the membrane capacitance. We are not interested in reproducing the detailed spike profile (which was achieved in Mahowald & Douglas, 1991). Rather, our goal is to reproduce the membrane-voltage trajectory during the interspike interval, as shaped by slow currents such as the Ca-dependent K current.

Eq. (2) captures the dependence of the K current on the membrane voltage's trajectory and on spiking activity. The first term models the dependence of the K current on the membrane voltage's temporal derivative, which is proportional to the net current supplied to the membrane capacitor (i.e.  $I_{in} - I_K$ ). The second term models Ca entering the cell

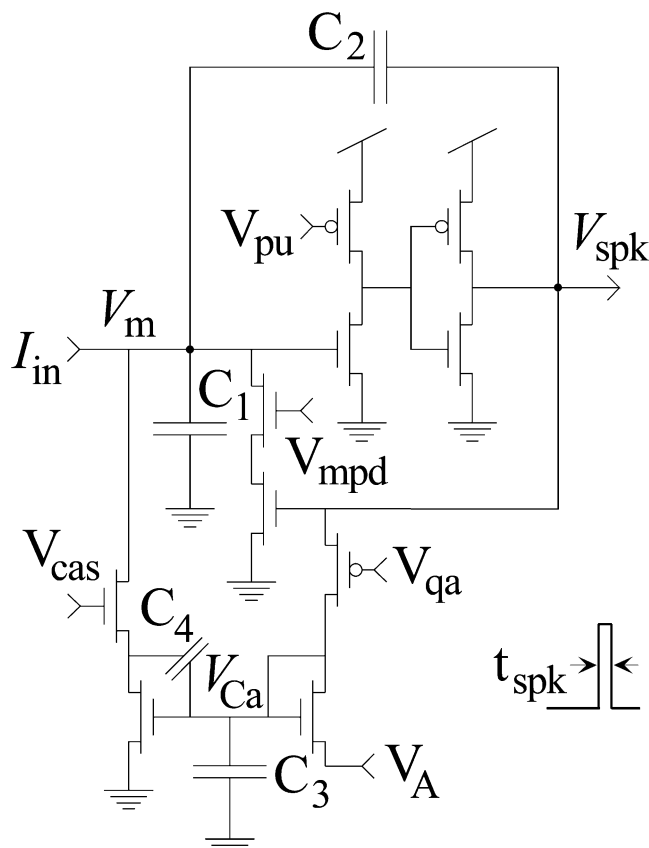


Fig. 4. AdaptSiNeuron's circuit. Two digital inverters, with capacitive positive feedback ( $C_2/C_1$ ), generate the spike. Two series-connected transistors, tied to  $V_m$ , terminate it. A pMOS transistor, with gate tied to  $V_{qa}$ , meters  $q_{ca}$  coulombs onto  $C_3$  each time a spike occurs. The drain-gate overlap capacitance of current-mirror's output transistor,  $C_4$ , is isolated from  $V_m$  by tying  $V_{cas}$ , which is normally tied high, to 1.35 V (plots in Fig. 2a were obtained this way). The circuit parameters are:  $r_{cm} \equiv C_4/(C_1 + C_2 + C_4)$ ,  $r_{mc} \equiv C_4/(C_3 + C_4)$ ,  $C_{Ca} \equiv C_3 + r_{cm}(C_1 + C_2)$ ,  $C_m \equiv C_1 + C_2 + r_{mc}C_3$ ,  $Q_{th} \equiv C_2 V_{dd}$ ,  $q_{Ca} \equiv I_{ds0} \exp((V_{dd} - \kappa V_{qa})/U_T) t_{spk}$ . The circuit layout is  $162 \times 108 \mu\text{m}^2$  in  $2 \mu\text{m}$ , double poly, double metal, p-well CMOS technology, made available through MOSIS.

each time a spike occurs. Part of this charge is lost when the membrane voltage is reset, hence the  $-r_{cm}Q_{th}$  term. The third term models buffering of Ca within the cell. Ca buffering can be canceled by a rising membrane voltage, as the temporal-derivative dependence mimics Ca influx, which is, indeed, the case in equilibrium.

Note that the K current turns on when the membrane voltage rises rapidly, and *stays* on at a steady level of depolarization—until Ca buffers reduce the intracellular-Ca concentration. Hence, the slow Ca dependence is the analog of the inactivation variable  $h$  used for the fast Na conductance in the Hodgkin–Huxley model. Slow inactivation is crucial for slow-rate adaptation because a sustained current is required to cancel the steady input current, so as to arrest the membrane voltage and hold it just below the threshold. Of course, the K current can still be turned off quickly by rapid hyperpolarization, through its voltage dependence.

For a constant input current, with  $I_{in}(t) = I_0$ , we can solve Eqs. (1) and (2) for the membrane voltage and K current trajectories in closed form (see Appendix B). Taking into account the exponential dependence of  $I_K$  on  $V_{Ca}$ , the resulting expressions for the trajectories during the interspike

interval from  $t_n$  to  $t_{n+1} = t_n + T_0$  are:

$$V_m(t) - V_m(t_n) = \frac{I_0}{C_m} \left( \eta \tau_0 \log \left( \frac{I_K(t)}{I_K(t_n)} \right) + (1 - \eta)(t - t_n) \right), \quad (3)$$

$$\frac{I_K(t)}{I_K(t_n)} = \frac{1}{(1 - \beta) \exp \left( -\frac{t - t_n}{\tau_0} \right) + \beta}, \quad (4)$$

Substituting the second equation into the first one yields an expression for the membrane voltage as a function of time that is an excellent fit to experimental measurements, as shown in Fig. 5a, where  $\tau_0$ ,  $\beta$ , and  $\eta$  are also defined. Notice that decoupling these equations by setting  $\eta = 0$  results in pure integrate-and-fire behavior.

AdaptSiNeuron's membrane voltage responds to a small step change in its input current, like the one used in Fig. 1, is shown in Fig. 5b. The spike latency is 10 ms in this particular example because the membrane voltage was arrested before it reached threshold. It would have escaped if it was closer to threshold at the time the step occurred. Indeed, for

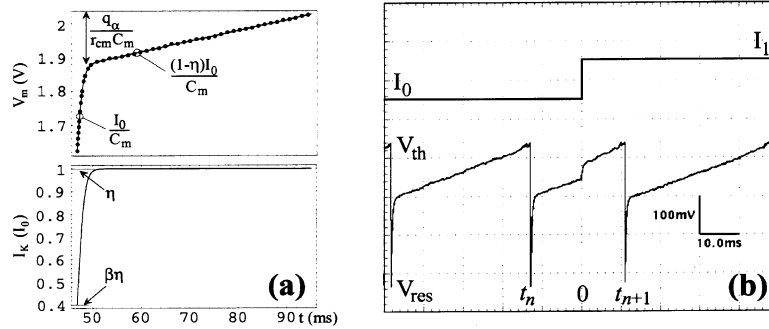


Fig. 5. AdaptSiNeuron's membrane trajectories. (a) Traces of membrane voltage ( $V_m$ ) and K current ( $I_K$ ), during an interspike interval, and two-slope approximation:  $I_0$  is the constant input current. Dots are measurements; lines are fits.  $\beta \equiv \exp((q_{Ca} - r_{cm}Q_{th})/Q_T)$  (0.400 for fit) is the fraction of  $I_K$  left when the membrane is reset.  $\eta \equiv r_{cm}(1 + r_{mc}/A)/(r_{cm} + 1/A)$  (0.9927) is the fraction of the input current drained away when  $I_K$  recovers and  $\tau_0 \equiv Q_T/r_{cm}I_0$  (0.654 ms) is  $I_K$ 's time constant;  $Q_T \equiv C_{Ca}U_T/\kappa$  is the amount of charge we must add to the Ca node to e-fold  $I_K(t)$ .  $V_m$  repolarizes to within  $q_{Ca}/r_{cm}C_m$  volts of threshold before  $I_K$  recovers completely (see Appendix C). (b) Effect of 2% step change in input current applied at the time indicated by the upper trace. This particular interspike interval is shortened by 35%, but the next one does not differ significantly from the previous one—35 and 37 ms, respectively. Spikes have been removed.

this 2% change, AdaptSiNeuron fires a spike with extremely short latency ( $<1$  ms) whenever we catch it in the last 20% or so of its interspike interval. This escape interval becomes a larger fraction of the interspike interval as the step size gets larger. The membrane escapes all the time if the current increases by more than a factor of  $\exp(q_{Ca}/Q_T)$ —the amount by which each spike multiplies the K current. Such large current steps invoke spike-rate adaptation.

Both spike-rate and slew-rate adaptation factors are proportional to the current-mirror's gain,  $A$  (see Appendix C), which sets the ratio between the Ca-decay and K-current time constants,  $\tau_{Ca}$  and  $\tau_0$ , because, increasing  $\tau_{Ca}$  reduces the slew rate, which, in turn, lengthens the interspike interval. The impact on the interspike interval is less if small Ca charge increments,  $q_{Ca}$ , are used, because the membrane voltage gets closer to threshold before it is arrested (see Fig. 5a). A stronger K-current voltage dependence (i.e. larger  $r_{cm}$ ) also improves slew-rate adaptation, because smaller voltage increases can compensate for inactivation through Ca decay. However, this decrease in slew rate has negligible effect on spike-rate adaptation because the membrane voltage switches to the slow slew rate closer to threshold.

#### 4. Extrapolated population responses

Theoretically, for a step change in input current from  $I_0$  to  $I_1$  that occurs at time  $t = 0$  (see Fig. 5a), we can show that the spike probability density will be

$$p(t_{n+1}) = \left( \frac{I_1}{I_0} + \xi \left( \frac{I_1}{I_0} - \frac{I_1}{(I_1 - I_0)\exp\left(\frac{-t_{n+1}}{\tau_1}\right) + I_0} \right) \right) \frac{1}{T_0}. \quad (5)$$

Notice that large slew-rate adaptation factors ( $\xi$ ) make the spike density extremely sensitive to fast changes in input

current. This gain is applied to the difference between the input current and the potassium current,  $I_K(t)$ , as demonstrated in Appendix D, where the above result is derived. Hence, the spike density is insensitive to DC input, or slow fluctuations, as these signals are canceled by  $I_K(t)$ , which is a low pass filtered version of the input current. Setting  $\xi = 0$  yields the result for Integrate&Fire, which is simply  $I_1/I_0T_0$ .

Experimentally, we can measure spike probability density using a single neuron by making a step change in its input current and measuring the latency of the first spike, repeating over several trials. The test neuron's state is randomized from trial to trial, just like for the asynchronous population state. Hence, when normalized by the number of trials, these single-neuron measurements recreate the spike probability density of an ensemble of identical neurons, which receive the same input, when they fire independently. Fig. 6a shows the results for AdaptSiNeuron; Fig. 6b shows the theoretical fit. As expected, the density peaks at zero latency and decays sigmoidally, in contrast with the pure exponential decay obtained with linear resistor–capacitor nerve-membrane models (Gerstner, 2000).

Starting with subpercent step amplitudes, we observe significant increases in the peak spike density (see Fig. 6a). This peaking is linearly proportional to step amplitude, and shifts the probability distribution to extremely short latencies. Thus, the fraction of the population that spikes in a submillisecond time window is proportional to the step amplitude—a degree-of-participation code—which has been named *space-rate* coding (Maass & Natschlag, 2000). Once the whole distribution has shifted to short latencies, we observe the impact of a shortening K channel time constant,  $\tau_1$ , which is inversely proportional to the new current level,  $I_1$ . This tightening pushes the peak up further. Now, all the neurons fire, but in shorter and shorter time windows for further increases in step amplitude—a degree-of-coincidence code (Diesmann, Gewaltig, & Aertsen, 1999).

AdaptSiNeuron's peak spike density increases much

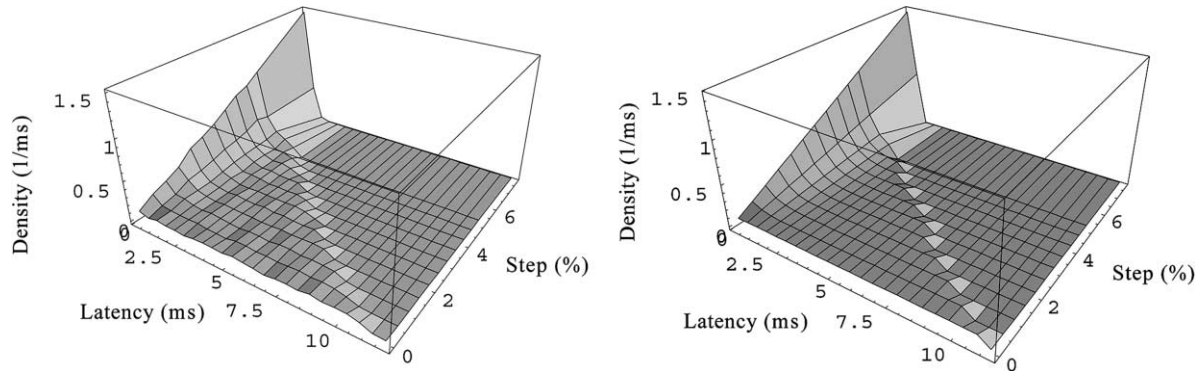


Fig. 6. Spike probability density. (a) Experimental latency measurements binned at 0.232 ms; 2000 trials were performed for each of 12 current step amplitudes. Biases were set to  $V_{qa} = 4.37$  V and  $V_A = 225$  mV. (b) Theoretical fits with  $\xi = 301.8$ ,  $T_0 = 11.0$  ms, and  $\tau_0 = 0.586$  ms.

faster than its spike rate does with step amplitude, as shown in Fig. 7. That is, step amplitudes of 0.51 and 3.5% double the peak density and the spike rate, respectively, based on theoretical fits to these measurements. The measured density will be even more sensitive if infinitesimally small bin sizes were used, instead of averaging the first 0.5 ms, as was the case in this data analysis. In theory, based on the value of  $\xi = 301.8$  used to fit the data, we expect a 0.33% change in the input to double the spike density at zero latency. Nevertheless, AdaptSiNeuron is much more sensitive than Integrate&Fire, which requires a 100% increase in input current to double either its spike density or spike rate.

Our theoretical results suggest that the slow-rate adaptation factor,  $\xi$ , determines how sensitive the spike density is to changes in input current. We investigated this directly with AdaptSiNeuron by changing the bias voltage  $V_A$ , which exponentially controls  $\xi$  (see Appendix C). Our results, shown in Fig. 8, show the expected exponential dependence (see Fig. 9), confirming the theory. Changing  $V_A$  from 205 to 265 mV changed the gain (i.e. ratio between the percentage changes in input current and spike density) from 104 to 1220. This increase was accompanied by a

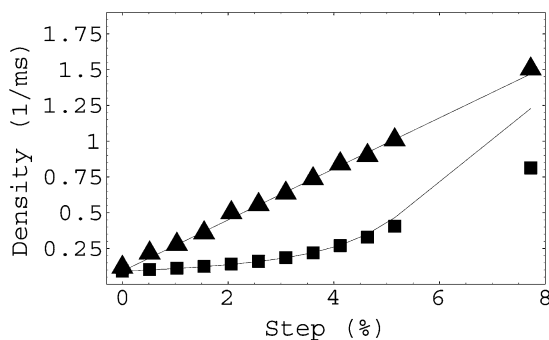


Fig. 7. Spike density versus spike rate. Spike density (triangles) in the first 0.5 ms bin and spike rate (squares) immediately after step (calculated from fitted parameter values), versus step amplitude, for the same data shown in Fig. 6a. Lines are theoretical results for  $t_{n+1} = 0.25$  ms and  $t_n = 0$ , respectively, using parameter values from the fit shown in Fig. 6b. A linear regression yields slopes of 17,900 and 2590  $s^{-1}$ , close to zero, with intercepts at 92.1 and 90.9  $s^{-1}$ , respectively.

decrease in baseline spike rate from 312 to 34.6 Hz, due to the dependence of the spike-rate adaptation factor,  $\gamma$ , on  $\xi$  (see Appendix C). We also confirmed that changing  $V_{Ca}$  over a range from 4.32 to 4.37 V, did not change the gain (data not shown), although it did change the baseline spike rate, from 32.0 to 90.4 Hz, due to the dependence of  $\gamma$  on  $q_{Ca}$ .

## 5. Discussion

Extrapolating our results to a neural population, with states randomized across the ensemble, just like the test neuron's state is randomized from trial to trial, we conclude that AdaptSiNeurons can fire in synchrony to encode step changes in their input currents linearly and immediately. Linearity and immediacy are possible because current determines flux—the rate at which neurons cross threshold (Knight, 1972). Abstractions that ignore actual spike timing, using differential equations to model the spike rate itself instead (Cohen & Grossberg, 1983; Hopfield, 1984; Wilson & Cowan, 1972), completely miss these features of the population spike density. Slow-rate adaptation, due to fast K-channel voltage dependence, make AdaptSiNeuron's spike density much more sensitive than its spike rate and its latency much shorter than its interspike interval—exceeding the performance of simple Integrate&Fire neurons analyzed previously (Gerstner, 2000; Knight, 1972).

Space-rate coding was originally motivated by the need to improve processing speed (Maass & Natschlagler, 2000) and a mechanism based on probabilistic synaptic transmission was proposed previously to achieve space-rate coding (Maass & Natschlagler, 2000). We have demonstrated here that random neuronal states can be exploited instead. If states are randomized, a different subset of the population is recruited each time, as only neurons that are close enough to threshold participate. However, in order to process a new input every interspike interval, the perturbed probability density must return to the uniform distribution rapidly. Unlike Integrate&Fire neurons, where the perturbation

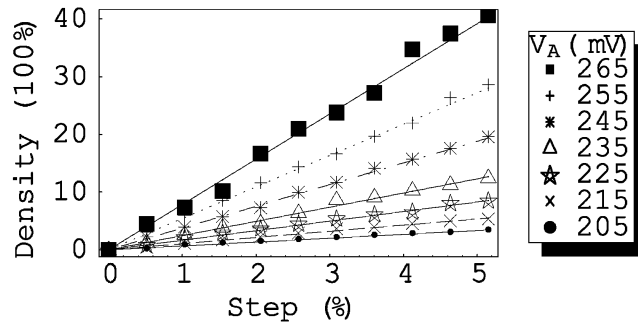


Fig. 8. Gain modulation. (a) Relative change in spike density versus relative change in current for seven values of  $V_A$  (see legend). A complete data set, like that shown in Fig. 7a, was obtained for each value of  $V_A$ , and fitted to obtain the lines in the plots.

persists indefinitely in the absence of noise (Gerstner, 2000), AdaptSiNeurons return to the asynchronous state on a submillisecond time scale—set by the potassium current’s voltage dependence (see Appendix D). As shown in Fig. 1, this complete randomization occurs for step sizes less than the amount by which the Ca increment boosts the potassium current. Thus, our approach has no throughput limitation for the range of current-step sizes over which space-rate coding occurs.

Attempts were made previously to improve the sensitivity of space-rate coding by suppressing fluctuations in the spike density using all-to-all inhibitory connections (Mar, Chow, Gerstner, Adams, & Collins, 1999). The improvement in sensitivity, which was dependent on population size, could be as high as two orders of magnitude for 1000 neurons. Our results suggest that cellular mechanisms can be used to achieve similar improvements in signal-to-noise ratio. Spike-rate adaptation attenuates noise, by reducing the background firing rate, and slew-rate adaptation amplifies signals coherently, by reducing the dependence of spike latency on neuronal state. Both forms of adaptation are realized just by adding active conductances to the simple Integrate&Fire model studied previously (Mar et al., 1999).

Our finding that slew-rate adaptation makes the spike density much more sensitive than the spike rate suggests that it may play a significant role in amplifying small signals. Indeed, primary neurons in the lateral lemniscus

of the central auditory pathway (Fu, Wu, Brezden, & Kelly, 1996) and in the lateral geniculate and medial habenular nuclei of the thalamus (McCormick, 1991; McCormick & Prince, 1987), as well as inhibitory interneurons in the CA1 region of the hippocampus (Fricker & Miles, 2000) and in the neocortex (Gupta, Wang, & Markram, 2000) display behavior similar to the slew-rate adaptation we have described here. In some instances, it was even demonstrated that slew-rate adaptation disappears when K conductances are blocked (Fricker & Miles, 2000; Fu et al., 1996), and that this led to a decrease in sensitivity and an increased latency (Fricker & Miles, 2000), as our model predicts.

Our finding that this sensitivity can be controlled by regulating voltage-dependent channels, Ca channels, or internal Ca buffers, suggests that slew-rate adaptation may play a role in gain modulation. There is evidence that the brain uses gain modulation to realize selective attention (Reynolds, Pasternak, & R, 2000), and that this increase in sensitivity is accompanied by increased synchrony (Steinmetz, Roy, Fitzgerald, Hsiao, Johnson, & Niebur, 2000), which is consistent with a slew-rate adaptation based mechanism. It is infeasible to change the gain, or sensitivity, of integrate&fire neurons, since this requires modifying the membrane capacitance. However, when active conductances are present, sensitivity can be increased by up-regulating voltage-dependent K channels or down-regulating Ca leakage or buffering to increase the slew-rate adaptation factor. Such regulation may happen through the action of neuromodulators, or through the action of metabotropic receptors, which can act much more rapidly.

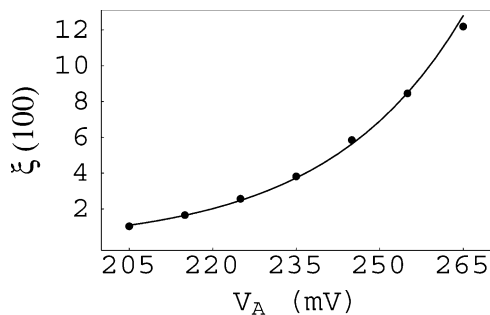


Fig. 9. Exponential adaptation factor dependence. Slew-rate adaptation factor,  $\xi$ , versus bias voltage.  $\xi$  was obtained from the slopes of the data fits in Fig. 8. The fit yields a thermal voltage of  $U_T = 24.3$  mV and voltage dependence ratio  $r_{cm} = 0.024$ .

#### Acknowledgements

We would like to acknowledge NSF’s LIS/KDI program (KDI-ECS98-74463) for support.

#### Appendix A. Diode-capacitor leaky integrator

The current-mirror integrator is shown in Fig. 3b; it is based on the well-known current-copying circuit. For



subthreshold current levels, the exponential current–voltage dependence makes the circuit nonlinear, so we cannot obtain a closed-form solution for any arbitrary input waveform. Instead, we derive an integral solution in this section.

The current-mirror integrator’s dynamic behavior is described by a simple differential equation:

$$C \frac{dV_{Ca}}{dt} = I_{Ca}(t) - I_d = I_{Ca}(t) - \frac{1}{A} I_K(t), \quad (6)$$

where  $A = \exp(V_A/U_T)$  is its current gain. The current passed by a MOS translator in saturation (i.e.  $V_d - V_s > 4 U_T$ ) is related to its gate and source voltages by  $I_{ds} = I_{ds0} \exp((\kappa V_g - V_s)/U_T)$ , in the subthreshold region. Hence, we can eliminate the voltage  $V_{Ca}$  and rewrite this equation solely in terms of the input and output currents:

$$Q_T \frac{d}{dt} \log\left(\frac{I_K(t)}{I_{ds0}}\right) = I_{Ca}(t) - \frac{1}{A} I_K(t), \quad (7)$$

where  $Q_T \equiv C U_T / \kappa$  is the amount of charge required to e-fold the current.

To gain insight into diode-capacitor dynamics, we rewrite the above differential equation in the following form:

$$\frac{Q_T}{I_{Ca}(t)} \frac{d(1/I_K)}{dt} = \frac{1}{A I_{Ca}(t)} - \frac{1}{I_K(t)}.$$

This equation is a simple first-order ordinary differential equation in  $1/I_K$  with ‘time constant’  $Q_T/I_{Ca}$ —which is fixed only if  $I_{Ca}(t)$  is constant. In that case, the difference  $1/I_K - 1/(A I_{Ca})$  decays like  $\exp(-t/\tau)$ , where  $\tau = Q_T/I_{Ca}$ .

If the input current is zero, multiplying both sides of the above equation by  $I_{Ca}(t)/Q_T$  reveals that:

$$\frac{d(1/I_K)}{dt} = \frac{1}{A Q_T} - \frac{1}{Q_T} \frac{I_{Ca}(t)}{I_K(t)}.$$

That is,  $1/I_K$  grows linearly at the rate  $1/(A Q_T)$  when  $I_{Ca}(t) = 0$ . Hence,  $I_K$  decays like  $1/t$ —the current gain,  $A$ , determines the one-over- $t$  decay rate. That is,

$$I_K(t) = \frac{1}{t/(A Q_T) + 1/I_K(0)}.$$

Now, we tackle the general case, for any arbitrary input waveform,  $I_{Ca}(t)$ . Integrating both sides of Eq. (7) from  $t_0$  to  $t$ , yields

$$\log\left(\frac{I_K(t)}{I_K(t_0)}\right) + \frac{1}{A Q_T} \int_{t_0}^t I_K(s) ds = \frac{1}{Q_T} \int_{t_0}^t I_{Ca}(s) ds,$$

after moving the  $I_K(t)$  term on the right to the left. Exponentiating both sides and integrating a second time from  $t_0$  to  $t$ , yields

$$\frac{A Q_T}{I_K(t_0)} \left| \exp\left(\frac{1}{A Q_T} \int_{t_0}^u I_K(s) ds\right) \right|_{u=t_0}^{u=t} = \int_{t_0}^t \exp\left(\frac{1}{Q_T} \int_{t_0}^u I_{Ca}(s) ds\right) du.$$

Evaluating the expression on the left at the limits,  $u = t_0$  (which equals 1) and  $u = t$ , moving the constant to the

other side, and taking the log of both sides yields

$$\begin{aligned} & \frac{1}{A Q_T} \int_{t_0}^t I_K(s) ds \\ &= \log\left(\frac{I_K(t_0)}{A Q_T} \int_{t_0}^t \exp\left(\frac{1}{Q_T} \int_{t_0}^u I_{Ca}(s) ds\right) du + 1\right). \end{aligned}$$

Finally, differentiating both sides yields

$$I_K(t) = A Q_T \frac{d}{dt} \log\left(\frac{I_K(t_0)}{A Q_T} \int_{t_0}^t \exp\left(\frac{1}{Q_T} \int_{t_0}^u I_{Ca}(s) ds\right) du + 1\right) \quad (8)$$

$$= \frac{\exp\left(\frac{1}{Q_T} \int_{t_0}^t I_{Ca}(s) ds\right)}{\frac{I_K(t_0)}{A Q_T} \int_{t_0}^t \exp\left(\frac{1}{Q_T} \int_{t_0}^u I_{Ca}(s) ds\right) du + 1} I_K(t_0). \quad (9)$$

## Appendix B. K current and membrane voltage trajectories

We can use the saturation current expression  $I_K = I_{ds0} \exp(\kappa V_{Ca}/U_T)$  to obtain a differential equation for  $I_K$  by eliminating  $V_{Ca}$  from Eq. (2). Thus, we obtain the following system of equations:

$$C_m \frac{dV_m}{dt} = I_{in} - r_{mk} I_K - (Q_{th} - r_{mc} q_{Ca}) \delta(t - t_n), \quad (10)$$

$$\frac{C_{Ca} U_T}{r_{cm} \kappa} \frac{d}{dt} \log\left(\frac{I_K(t)}{I_{ds0}}\right) = I_{in} - \frac{r_{ck}}{r_{cm}} I_K - (Q_{th} - q_{Ca}/r_{cm}) \delta(t - t_n). \quad (11)$$

We introduced the factor  $r_{mk} \equiv 1 + r_{mc}/A$  to account for current discharging the membrane capacitor and the factor  $r_{ck} \equiv r_{cm} + 1/A$  to account for current discharging the calcium capacitor. The two additive terms describe components that arise from the potassium-channel transistor or the diode-connected transistor, and crossover from one capacitor to the other through  $C_4$ ; both are proportional to  $I_K(t)$ .

To solve for the membrane voltage trajectory, in integral form, we express  $I_K(t)$  in terms of its derivative, using Eq. (11), and substitute this expression into Eq. (10). Integrating over time, starting at  $t_n$ , the time that the last spike occurred, yields:

$$V_m(t) - V_m(t_n) = \eta \frac{Q_{Tm}}{C_m} \log\left(\frac{I_K(t)}{I_K(t_n)}\right) + (1 - \eta) \frac{1}{C_m} \int_{t_n}^t I_m(r) dr, \quad (12)$$

where  $Q_{Tm} \equiv C_{Ca} U_T / (\kappa r_{cm})$  is the amount of charge we must add to the membrane node to e-fold  $I_K(t)$ ,  $I_m(t) \equiv I_{in}(t) - (Q_{th} + A q_{Ca}) \delta(t - t_{n+1})$  is the current supplied to the membrane node, and  $\eta \equiv r_{mk} r_{cm} / r_{ck}$  is the fraction of this current that is drained away.

To solve for the potassium current trajectory, observe that its differential equation (11) is homologous with that for the current-mirror integrator (Eq. (7)), with the following

analogies:

$$\frac{C_{Ca}U_T}{r_{cm}\kappa} \leftrightarrow Q_T,$$

$$\frac{r_{cm}}{r_{ck}} \leftrightarrow A,$$

$$I_{in}(t) - (Q_{th} - q_{Ca}/r_{cm})\delta(t - t_n) \leftrightarrow I_{Ca}(t).$$

Hence, we can use our general integral solution for the current-mirror integrator (Eq. (9)) to obtain the potassium current's response to any arbitrary time-varying current,  $I_{Ca}(t)$ , supplied to the calcium capacitor. The result is:

$$I_K(t) = \frac{\exp\left(\int_{t_n}^t \frac{I_{Ca}(s)}{Q_{Tm}} ds\right)}{\frac{r_{ck}I_K(t_n)}{r_{cm}Q_{Tm}} \int_{t_n}^t \exp\left(\int_{t_n}^u \frac{I_{Ca}(s)}{Q_{Tm}} ds\right) du + 1} I_K(t_n). \quad (13)$$

For the AdaptSiNeuron circuit,  $I_{Ca}(t) \equiv I_{in}(t) - (Q_{th} - q_{Ca}/r_{cm})\delta(t - t_{n+1})$  and, for the special constant current case (i.e.  $I_{in}(t) = I_0$ ), we can readily evaluate the integrals in Eqs. (12) and (13). The results are given in the text (Eqs. (3) and (4)).

### Appendix C. Adaptation factors

To compute the slew-rate adaptation factor, we compare how fast the input current charges the membrane capacitance with how fast it charges after the potassium current turns on and steals a fraction  $\eta$  of the input (see Fig. 5a). We have:

$$\xi \equiv \frac{I_0}{C_m} / \left. \frac{dV_m}{dt} \right|_{t=t_1} - 1 = \frac{\eta}{1 - \eta} = r_{cm} \frac{A + r_{cm}}{1 - r_{cm}r_{mc}} \quad (14)$$

where  $t = t_1$  at the end of the interspike interval. This adaptation factor is achieved in practice only if the potassium-channel current is virtually shut off when the membrane voltage is reset. If the residual fraction  $\beta$  of the potassium current is not negligible, the actual slew-rate adaptation drops by a factor of  $(1 - \beta)$ . For the fit shown in Fig. 5a, this approximation predicts  $\xi = 84.1$  from the fitted values of  $\eta$  and  $\beta$ , which is pretty close to the value of  $\xi = 78.9$  obtained by measuring the slew rates directly.

To compute the spike-rate adaptation factor, we use the two-slope approximation for the membrane voltage trajectory shown in Fig. 5a. However, first, we need to know how close the membrane voltage is to threshold when it switches to the slow slew rate. Let us assume that this happens when  $I_K(t)$  returns to the level it had before the membrane voltage was reset. Hence, the shortfall in the membrane voltage must exactly cancel the charge,  $q_{Ca}$ , added to the calcium capacitor by the spike to boost  $I_K(t)$ . This intuition leads us to conclude that the voltage shortfall is  $q_{Ca}/(r_{cm}C_m)$ , as shown in Fig. 5a, taking into account the capacitive-divider ratio  $r_{cm}$ .

Hence, switching to a slow slew rate is equivalent to

elevating the threshold by  $\xi q_{Ca}/(r_{cm}C_m)$ , as the membrane voltage changes  $1 + \xi$  times more slowly over the last  $q_{Ca}/(r_{cm}C_m)$  volts. Thus, the period becomes  $(Q_{th} + \xi q_{Ca}/r_{cm})/Q_{th}$  times longer. Therefore, the spike-rate adaptation factor,  $\gamma$ , is related to the slew-rate adaptation factor,  $\xi$ , by

$$\gamma \equiv \frac{T_0}{Q_{th}/I_0} - 1 = \frac{\xi}{r_{cm}} \frac{q_{Ca}}{Q_{th}} = \frac{A + r_{mc}}{1 - r_{cm}r_{mc}} \frac{q_{Ca}}{Q_{th}} \quad (15)$$

as the steady-state interspike interval,  $T_0$ , is  $(Q_{th} + \xi q_{Ca}/r_{cm})/I_0$ , but would be  $Q_{th}/I_0$  without adaptation.<sup>1</sup>

### Appendix D. Spike density

The time-scaling ratio,  $dt_n/dt_{n+1}$ , is all we need to know to compute how an adapted neuron's spike density is reshaped by its input current. This function tells us exactly how much to shrink or stretch time intervals as we map spikes from  $t_n$  to  $t_{n+1}$  (see Fig. 5b). By our definition, a neuron is adapted if its behavior only depends on the most recent spike. That is, its state at time  $t$  is entirely determined by the time elapsed since it last spiked,  $t - t_n$ . In that case, we can determine the spike probability density for a population of identical neurons,  $p(t_{n+1})$ , at time  $t_{n+1}$ , if we know the density,  $p(t_n)$ , at time  $t_n$ .

To show how  $dt_n/dt_{n+1}$  is related to the spike density  $p(t_{n+1})$ , let  $dt_n$  be a time interval starting at  $t_n$  and let  $dt_{n+1}$  be a time interval starting at  $t_{n+1}$ . Demarcate the second interval such that in each case where a spike occurs in the first interval, then it is followed by a spike that falls in the second interval—spikes are conserved. Thus, we must have

$$dt_{n+1}p(t_{n+1}) = dt_n p(t_n) \Rightarrow p(t_{n+1}) = \frac{dt_n}{dt_{n+1}} p(t_n). \quad (16)$$

Notice that higher time-scaling ratios yield higher spike densities.

To derive the time-scaling ratio,  $dt_n/dt_{n+1}$ , observe that no net charge can be supplied to the membrane capacitor over a complete cycle. Hence, if the last spike is shifted by  $dt_n$ , then the next spike must be shifted by  $dt_{n+1}$  to compensate for the amount of charge lost—charge is conserved. Thus, we must have:

$$dt_{n+1}I(t_{n+1}) = dt_n I(t_n) \Rightarrow \frac{dt_n}{dt_{n+1}} = \frac{I(t_{n+1})}{I(t_n)}, \quad (17)$$

where  $I(t)$  is the net current flowing into the membrane capacitance at any time  $t$ . In the case of AdaptSiNeuron,

<sup>1</sup> Alternatively, we can solve for the steady-state interspike interval  $T_0$  by imposing the adaptation condition  $I_K(t_1^-) = I_K(t_0^+)/\beta$ , between the potassium current levels at the beginning and the end of the interspike interval, on Eq. (3), and setting  $V_m(t_1^-) - V_m(t_0^+) = Q_{th}/C_m$ , where  $t_1 \equiv t_0 + T_0$  is the time the next spike occurs and  $\beta \equiv \exp((q_{Ca} - r_{cm}Q_{th})/Q_T)$ . This rigorous approach yields the same result.

this yields

$$\frac{dt_n}{dt_{n+1}} = \frac{I_{in}(t_{n+1}) - r_{mk}I_K(t_{n+1})}{I_{in}(t_n) - r_{mk}I_K(t_n)}, \quad (18)$$

as the factor  $r_{mk} \equiv 1 + r_{mc}/A$  accounts for both  $I_K(t)$  and the current through  $C_4$ . Given the input current waveform,  $I_{in}(t)$ , and the initial condition,  $I_K(t_n)$ , we can use Eq. (13) to compute  $I_K(t_{n+1})$ .

Now, let us consider a cycle starting just before the time,  $t_n$ , that the last spike occurred and let us assume that  $I_K(t)$  has reached steady state at the starting point (i.e.  $I_K(t_n) = r_{cm}I_0/r_{ck}$ , from Eq. (11)). In that case, Eq. (18) gives us

$$\begin{aligned} \frac{dt_n}{dt_{n+1}} &= \frac{I_{in}(t_{n+1}) - r_{mk}I_K(t_{n+1})}{I_0 - \eta I_0} \\ &= (1 + \xi) \frac{I_{in}(t_{n+1}) - r_{mk}I_K(t_{n+1})}{I_0}, \end{aligned} \quad (19)$$

using the definitions  $\eta \equiv r_{mk}r_{cm}/r_{ck}$  and  $\xi \equiv \eta/(1 - \eta)$  (see Appendix C). This result applies if the input current remains constant sufficiently long, as is the case for sparse sporadic synaptic inputs superimposed on a constant background current level.

For a step change in the input current from  $I_0$  to  $I_1$ , we can readily compute  $I_K(t_{n+1})$  from Eq. (13). If we assume  $I_K(t)$  is in steady state when the step occurs, we obtain

$$I_K(t_{n+1}) = \frac{r_{cm}/r_{ck}}{\left(\frac{1}{I_0} - \frac{1}{I_1}\right)\exp\left(-\frac{t_{n+1}}{\tau_1}\right) + \frac{1}{I_1}}, \quad (20)$$

assuming the step occurred at  $t = 0$ . To obtain the spike density, we substitute this result into Eq. (19), and then multiply by  $p(t_n)$ , which equals  $1/T_0$  if spikes are uniformly distributed. Thus, we obtain the result given in the text (Eq. (5)). This result applies only if the step occurs in the slow slew-rate phase of the membrane voltage's trajectory, as shown in Fig. 5b, due to the steady-state assumption.

Finally, we need to determine where the distribution cuts off, which requires us to compute the maximum latency,  $\hat{T}_1$ . To do this, we integrate  $p(t_{n+1})$  from 0 to  $\hat{T}_1$  and equate the result to 1. Thus, we obtain

$$T_0 = \frac{I_1}{I_0} \hat{T}_1 - \xi \tau_0 \log\left(\frac{I_1 - I_0}{\tau_1} \exp\left(-\frac{\hat{T}_1}{\tau_1}\right) + \frac{I_0}{I_1}\right), \quad (21)$$

after substituting  $\tau_0 = (I_1/I_0)\tau_1$ . We solved this equation numerically to obtain  $\hat{T}_1$ , after substituting the values of  $\xi$  and  $\tau_0$  used to fit Eq. (5) to the density measurements;  $T_0$  was determined by measuring the density in the absence of a

step. As  $\hat{T}_1$  is equal to the interspike interval immediately after the step, we used its reciprocal to obtain the spike-rate fit shown in Fig. 7. This result overestimates the spike rate at large step sizes because of the steady-state assumption, which effectively ignores the fast slew-rate phase when the membrane is further away from the threshold, leading to shorter estimates for the interspike interval.<sup>2</sup>

By repeating this procedure, to relate  $p(t_{n+2})$  to  $p(t_{n+1})$ , we can determine how quickly the perturbation in the spike density disappears. We have

$$\begin{aligned} p(t_{n+2}) &= \frac{I_{in}(t_{n+2}) - r_{mk}I_K(t_{n+2})}{I_{in}(t_{n+1}) - r_{mk}I_K(t_{n+1})} p(t_{n+1}) \\ &= \frac{I_{in}(t_{n+2}) - r_{mk}I_K(t_{n+2})}{I_{in}(t_n) - r_{mk}I_K(t_n)} \frac{1}{T_0}, \end{aligned} \quad (22)$$

using Eqs. (16) and (18), and setting  $p(t_n) = 1/T_0$ . The net-current ratio evaluates to  $I_1/I_0$  if  $I_K(t)$  is in steady state when  $t = t_{n+2}$  as well as when  $t = t_n$ . Given that the K-current trajectory is similar to that in Eq. (20), the density becomes uniform for  $t_{n+2} > t_{n+1} + 4\tau_1$ —a time period much shorter than the interspike interval.

## References

- Alonso, J. M., Usrey, W. M., & Reid, R. C. (1996). Precisely correlated firing in cells of the lateral geniculate nucleus. *Nature*, 383 (6603), 815–819.
- Boahen, K. (1997). The retinomorph approach: pixel-parallel adaptive amplification, filtering, and quantization. *Analog Integr. Circ. Sig. Proc.*, 13, 53–68.
- Buracas, G. T., Zador, A. M., DeWeese, M. R., & Albright, T. D. (1998). Efficient discrimination of temporal patterns by motion-sensitive neurons in primate visual cortex. *Neuron*, 20 (5), 959–969.
- Cohen, M. A., & Grossberg, S. (1983). Absolute stability of global pattern formation and parallel memory storage by competitive neural networks. *IEEE Transactions on Systems, Man, and Cybernetics*, 13, 815–823.
- Connor, J. A., & Stevens, C. F. (1971). Voltage clamp studies of transient outward membrane current in gastropod neural stomata. *J. Physiol.*, 213 (1), 21–30.
- Dan, Y., Alonso, J. M., Usrey, W. M., & Reid, R. C. (1998). Coding of visual information by precisely correlated spikes in the lateral geniculate nucleus. *Nature Neuroscience*, 1 (6), 501–507.
- deCharms, R. C., & Zador, A. (2000). Neural representation and the cortical code. *Annual Review of Neuroscience*.
- Diesmann, M., Gewaltig, M. O., & Aertsen, A. (1999). Stable propagation of synchronous spiking in cortical neural networks. *Nature*, 402 (6761), 529–533.
- Fricker, D., & Miles, R. (2000). EPSP amplification and the precision of spike timing in hippocampal neurons. *Neuron*, 28, 559–569.
- Fu, X. W., Wu, S. H., Brezden, B. L., & Kelly, J. B. (1996). Potassium currents and membrane excitability of neurons in the rat's dorsal nucleus of the lateral lemniscus. *J. Neurophysiol.*, 76 (2), 1121–1132.
- Gerstner, W. (1999). *Pulsed neural networks*, Cambridge, MA: MIT Press.
- Gerstner, W. (2000). Population dynamics of spiking neurons: fast transients, asynchronous states, and locking. *Neural Computation*, 12 (1), 43–89.
- Gupta, A., Wang, Y., & Markram, H. (2000). Organizing principles for a diversity of gabaergic interneurons and synapses in the neocortex. *Science*, 287, 273–278.

<sup>2</sup> An exact relationship between  $t_{n+1}$  and  $t_n$  can be derived by substituting the general solution for  $I_K(t)$  (Eq. (13)) into the membrane voltage equation (Eq. (12)) and evaluating integrals over the interspike interval, stepping the input current from  $I_0$  to  $I_1$  at  $t = 0$ . Differentiating this result implicitly yields an exact equation for  $dt_n/dt_{n+1}$ . A precise value of  $I_K(t_n^+)$  can be obtained by imposing the adaptation condition,  $I_K(t_1^-) = I_K(t_0^+)/\beta$ , on the constant-input solution for  $I_K(t)$  given by Eq. (13).

- Hodgkin, A. L., & Huxley, A. F. (1952). A quantitative description of membrane current and its application to conduction and excitation in nerve. *J. Physiol.*, 117, 500–544.
- Hopfield, J. J. (1984). Neurons with graded responses have computational properties like those of two-state neurons. *Proc. Natl. Acad. Sci. USA*, 81, 3088–3092.
- Knight, B. W. (1972). Dynamics of encoding in a population of neurons. *J. Gen. Physiol.*, 59 (6), 734–766.
- Lancaster, B., & R. A. P. (1986). Calcium-dependent current generating the after-hyperpolarization of hippocampal neurons. *J. Neurophysiol.*, 55, 1268–1282.
- Maass, W., & Natschlager, T. (2000). A model of fast analog computation based on unreliable synapses. *Neural Computation*, 12 (7), 1679–1704.
- Madison, D. V., & Nicoll, R. A. (1982). Noradrenaline blocks accommodation of pyramidal cell discharge in the hippocampus. *Nature*, 299 (5884), 636–638.
- Mahowald, M., & Douglas, R. (1991). A silicon neuron. *Nature*, 354 (6354), 515–518.
- Mainen, Z. F., & Sejnowski, T. J. (1995). Reliability of spike timing in neocortical neurons. *Science*, 268 (5216), 1503–1506.
- Mar, D. J., Chow, C. C., Gerstner, W., Adams, R. W., & Collins, J. J. (1999). Noise shaping in populations of coupled model neurons. *Proc. Natl. Acad. Sci. USA*, 96, 10450–10455.
- McCormick, D. A. (1991). Functional properties of slowly inactivating potassium current in guinea pig dorsal lateral geniculate relay neurons. *J. Neurophysiol.*, 66 (4), 1176–1189.
- McCormick, D. A., & Prince, D. A. (1987). Acetylcholine causes rapid nicotinic excitation in the medial habenular nucleus of guinea pig, in vitro. *J. Neurosci.*, 7 (3), 742–752.
- Mead, C. A. (1989). *Analog VLSI and neural systems*, Reading, MA: Addison-Wesley.
- Reynolds, J. H., Pasternak, T., & R. D. (2000). Attention increases sensitivity of v4 neurons. *Neuron*, 26 (3), 703–714.
- Steinmetz, P. N., Roy, A., Fitzgerald, P. J., Hsiao, S. S., Johnson, K. O., & Niebur, E. (2000). Attention modulates synchronized neuronal firing in primate somatosensory cortex. *Nature*, 404 (6774), 187–190.
- Storm, J. F. (1988). Temporal integration by a slowly inactivating K current in hippocampal neurons. *Nature*, 336, 379–381.
- Thorpe, S., Fize, D., & Marlot, C. (1996). Speed of processing in the human visual system. *Nature*, 381 (6582), 520–522.
- Wilson, H. R., & Cowan, J. D. (1972). Excitatory and inhibitory interactions in localized populations of model neurons. *Biophysical Journal*, 12, 1–24.